Pairing Combustion Experiments and Thermogravimetric Analysis to Uncover Timescales Controlling Cellulose Ignition and Burnout in a Hencken Burner

Parvaneh Motiei[a], Matteo Pecchi[b], James L. Adair[b], Jillian L. Goldfarb[b]
Jacqueline O'Connor[a,*]
[a] Mechanical Engineering, Pennsylvania State University, University Park, PA USA
[b] Biological and Environmental Engineering, Cornell University, Ithaca, NY USA

1 Thermogravimetric Analysis

Figure 1 shows the proximate analysis of cellulose in an inert atmosphere (N_2) and initial moisture/final ash measurements in an oxidative atmosphere (air) with varied heating rates. The proximate analysis indicates that microcrystalline cellulose is comprised of 0.2 ± 0.3 %(wt) ash, 92.9 ± 0.6 % volatile matter, and 6.9 ± 0.4 % fixed carbon. The oxidative runs show that heating rate has insignificant effects on measured starting moisture and final ash. The mean Thermogravimetric (TG) standard deviation indicates the average standard deviation across TG curves in replicates, and it is used to indicate reproducibility.

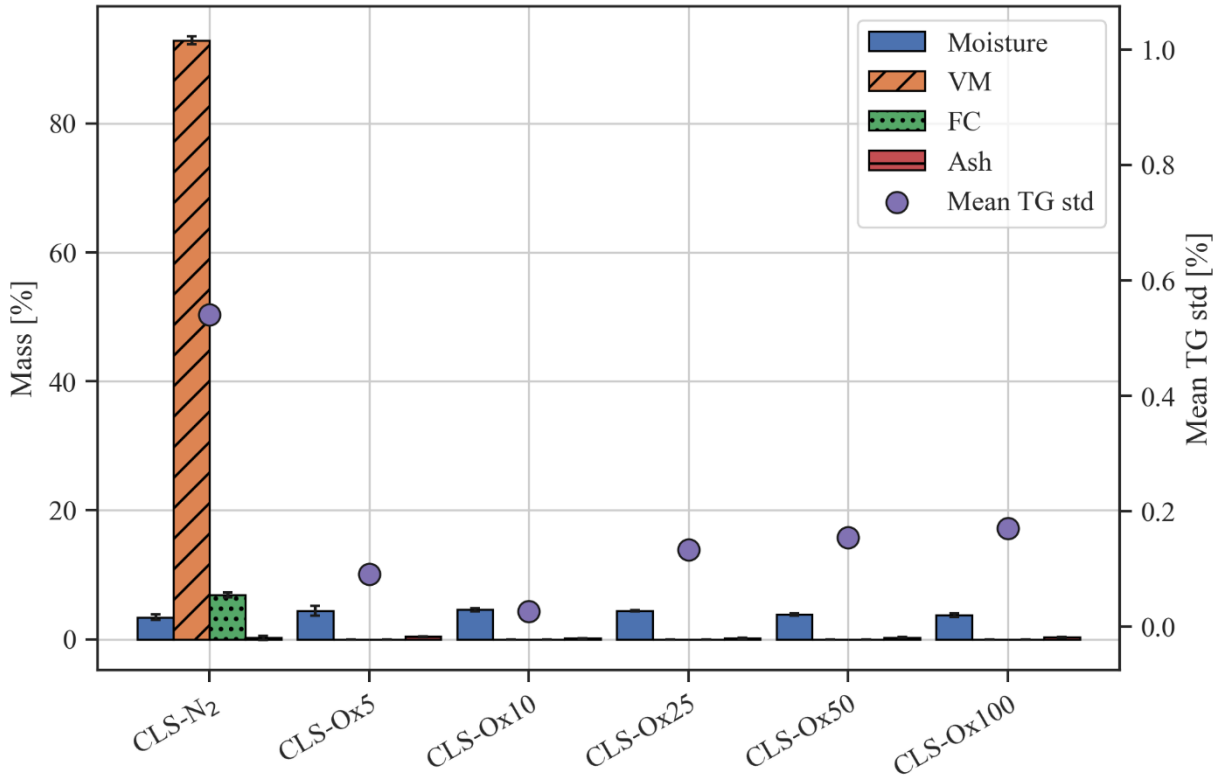

Figure 1. Proximate analysis of cellulose in an inert atmosphere (CLS-N2) and moisture/ash measurements in an oxidative atmosphere (CLSOx#, where # is heating rate in K/min).

Figure 2 shows the limitation of TG to show combustion behavior given the reliance on heating rate. On the left we plot the fraction of cellulose remaining in the crucible as a function of reaction time and on the right as a function of TGA furnace temperature in an air environment.

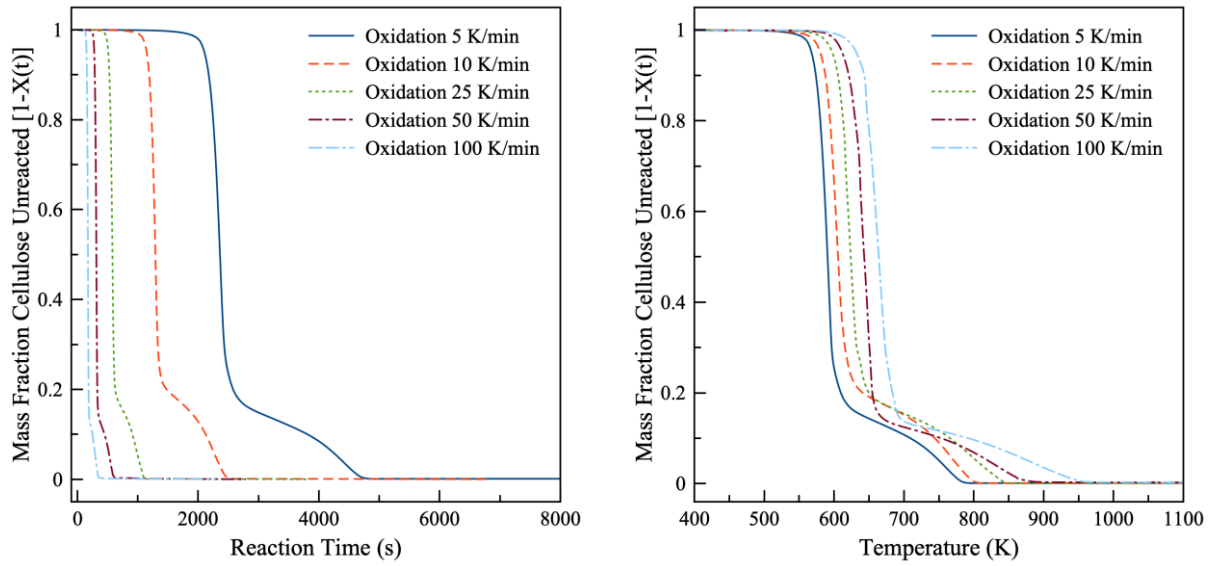

(a) **(b)**

Figure 2. TG results of cellulose plotted as Normalized mass loss [1-X(t)] where X(t) is the mass fraction remaining at any one time as a function of (b) time and (b) furnace temperature for oxidation of microcrystalline cellulose at five heating rates in an air environment.

Figure 3 enhances our discussion of the dependence of TG-calculated combustion properties on heating rate. We note a logarithmic dependence on heating rate for the ignition temperature and burn-out temperature.

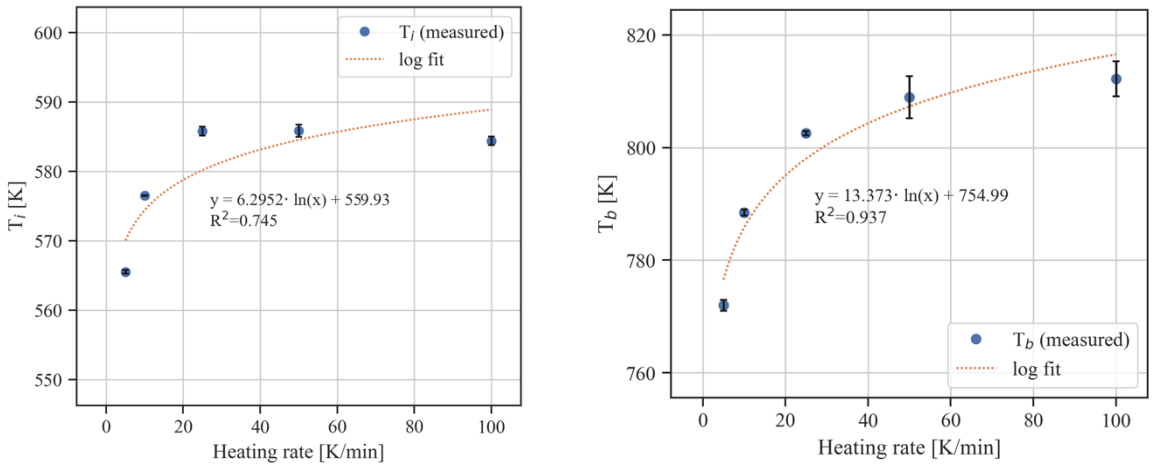

(a) **(b)**

Figure 3. Dependence of TG-measured combustion parameters (a) Ignition Temperature, T_i and (b) Burnout Temperature, T_b, on heating rate

2 Chemiluminescence Imaging

Figure 4 shows an example of a time-averaged CH* chemiluminescence image of cellulose particle combustion and the corresponding centerline signal intensity profile versus the height above the burner surface for 100 images, where each axial signal intensity corresponds to each individual image in 100 image set. Though there is some variation in the intensity and shape of the centerline chemiluminescence signal throughout the data collection period, the signal is relatively consistent throughout, an indication of consistent fluidization and burning through the duration of the experiment.

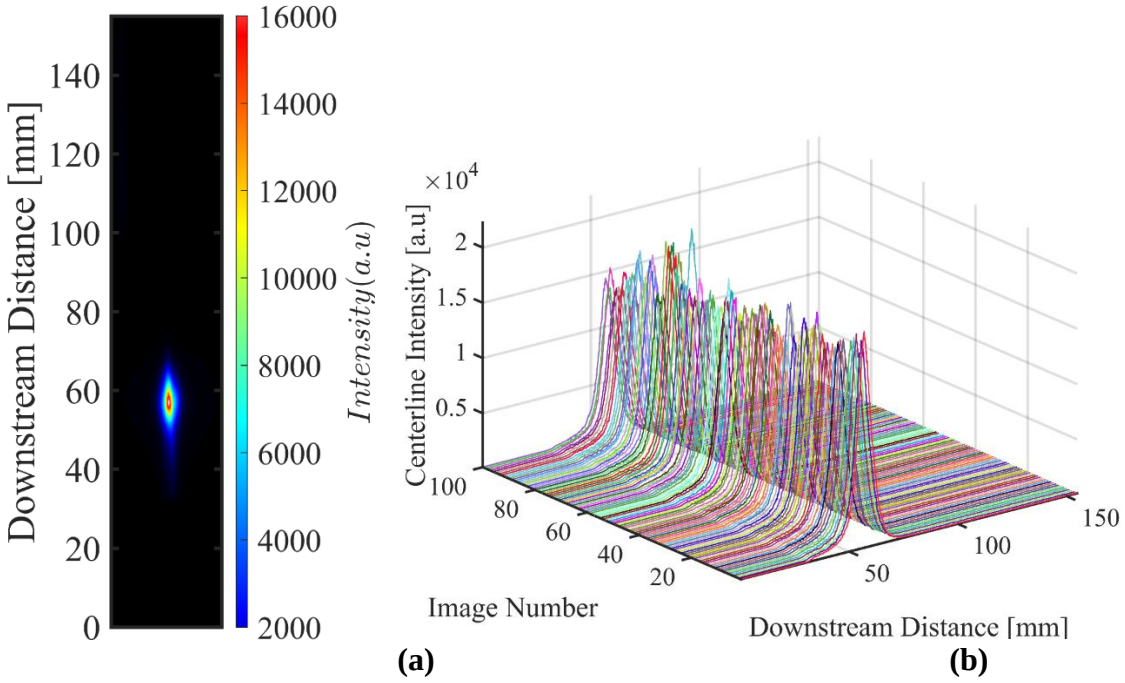

Figure 4. Example of a) time-averaged CH* chemiluminescence image of cellulose particles and b) intensity signal of the centerline for cellulose particles from CH* chemiluminescence for 100 separate images in the H_2/air test matrix at $\phi = 0.4$.

3 Repeatability testing in the H_2/air mixtures

Statistical repeatability tests were carried out on both CH* chemiluminescence imaging and velocity measurements from PIV. Six different CH* image datasets taken over multiple days for each condition and were processed to determine two quantities used in the calculation of the ignition delay time and volatile burning time: the ignition location, which is where the centerline CH* intensity equals 50% of the peak signal intensity, and the volatile burnout distance, which is the FWHM of the centerline signal. In the present study, we use the median as the measure of central tendency and the inner-quartile range (IQR) as a measure of statistical dispersion. Boxplots of an example condition, $\phi = 0.4$, are shown in Figure 5. The median is indicated by the red horizontal line and the inner-quartile range is indicated by the extent of the blue boxes. The black horizontal lines above and below the blue boxes indicate the maximum and minimum values of each data set, and the red crosses are outliers, which are defined as points greater than 1.5×IQR

from the median. The overlapping IQR indicates that the difference among datasets is not statistically significant.

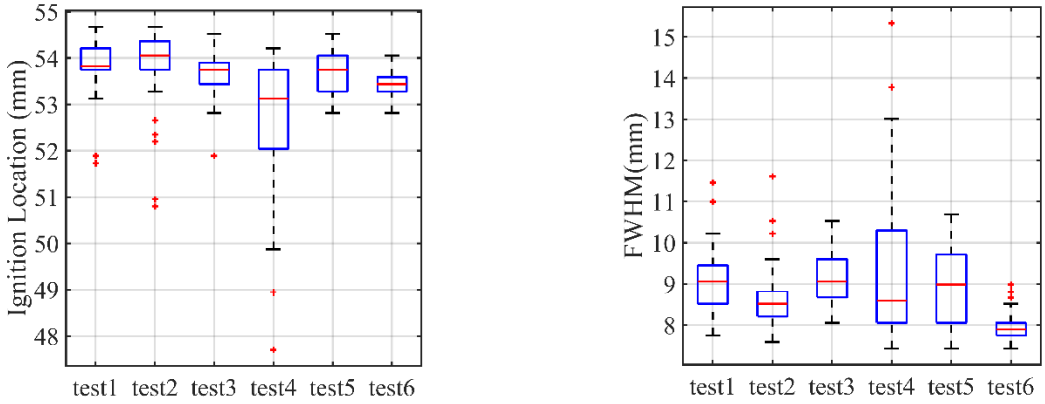

(a) **(b)**

Figure 5. Boxplots for six repeated tests of (a) ignition location and (b) FWHM for the H_2/air test matrix at $\phi = 0.4$.

The repeatability of the velocity measurements was also tested across multiple days; Figure 6 shows the results of five repeated tests for an example condition in the H_2/air test matrix, ϕ = 0.4, all of which are quantitatively similar. Similar repeatability was ensured in all cases. The ignition and the end of volatile burning locations obtained from CH* chemiluminescence imaging are shown by red vertical lines in the figure.

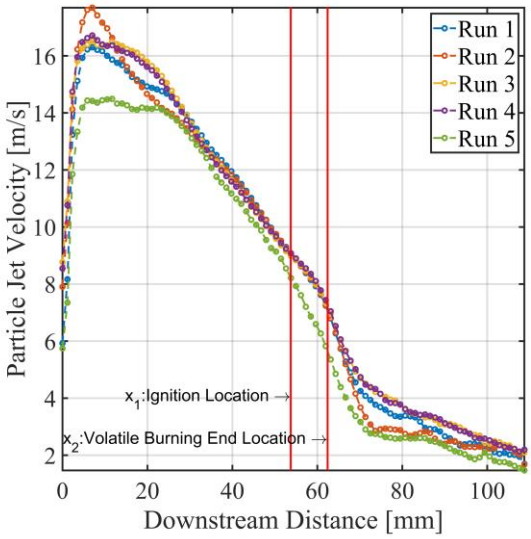

Figure 6. Cellulose particle velocity profile along the downstream distance for five different repeats of the H_2/air test matrix at $\phi = 0.4$.

4 Repeatability in O_2/N_2 mixtures

Statistical repeatability tests were performed for both CH* chemiluminescence imaging and particle velocity determined by PIV for the mixture with a reactant mole fraction of 0.21 O_2. Similar to the repeatability test in the H_2/air tests, the six repeats were performed over two days

with 100 images at each dataset. The measured FWHM and ignition location for all tests are shown in Figure 7, showing a satisfactory level of repeatability among different tests.

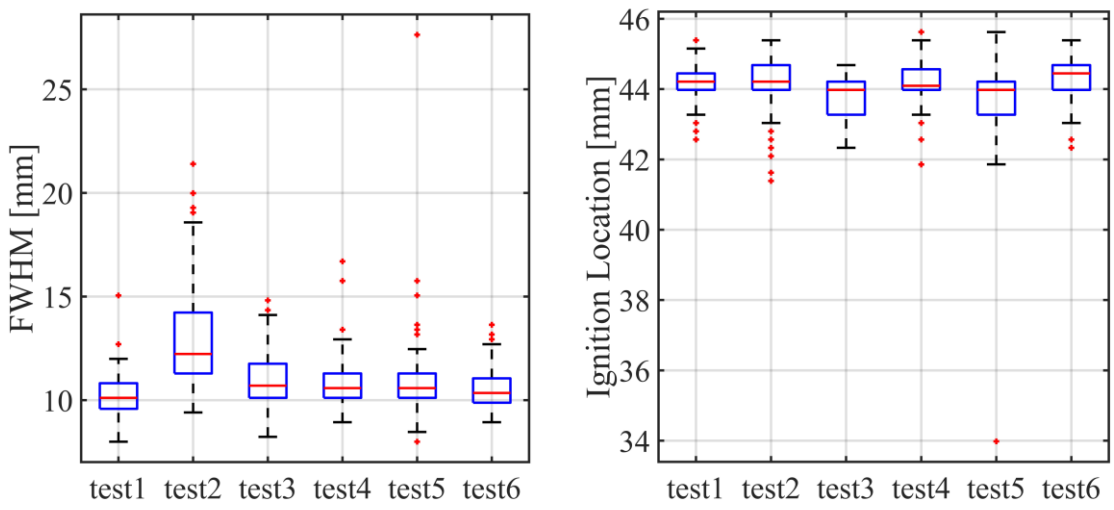

(a) **(b)**

Figure 7. Boxplots for (a) FHWM and (b) ignition location for mixture of 0.21 reactant oxygen mole fraction.

Figure 8 shows the corresponding velocity measurements of the six tests shown in Figure 7, as well as the median of the ignition locations and volatile burning end locations of the combined six datasets (600 samples) taken by CH* imaging.

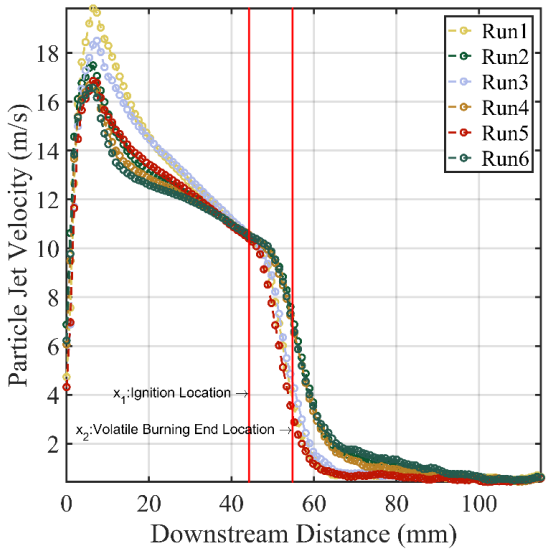

Figure 8. Particle velocity profile along the downstream distance for mixture of 0.21 O_2.

5 Key combustion length scales

Imaging of the particle combustion in air for each condition in the H_2/air test matrix is shown in Figure 9. The stand-off distance of the flame from the base of the burner decreases with increasing equivalence ratio, likely a result of the higher co-flow temperatures. The downstream

extent from the burner also decreases with increasing equivalence ratio, indicating more rapid burnout of the fuel at the higher co-flow temperatures.

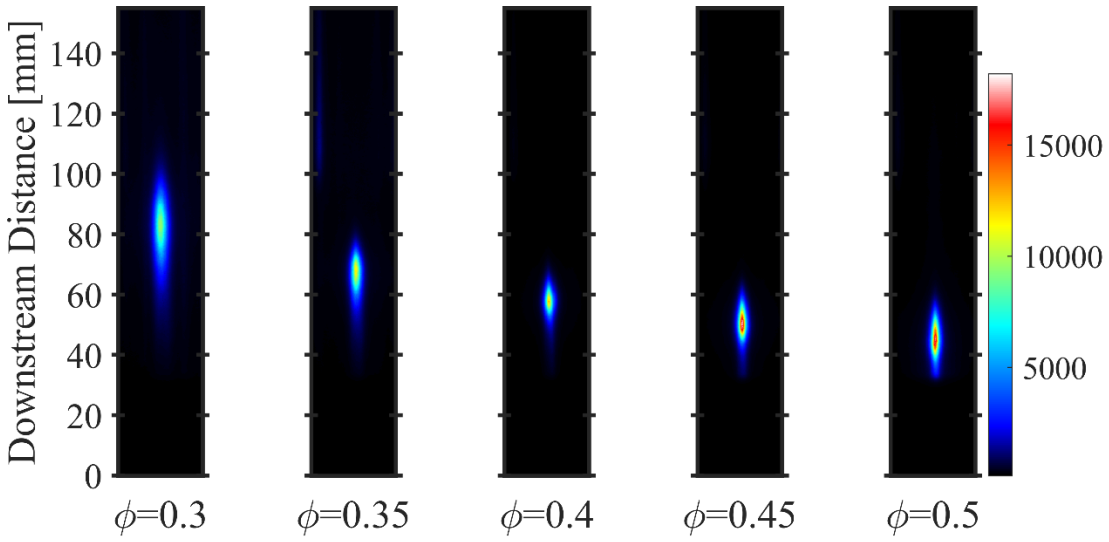

Figure 9. Time-averaged images of CH* chemiluminescence from cellulose at five equivalence ratios.

Figure 10 shows the time-averaged CH* chemiluminescence images for the constant-temperature, varying O_2 mole fraction cases in the O_2/N_2 test matrix; the centerline profiles of these time-averaged images are shown in Figure 6 of the main manuscript.

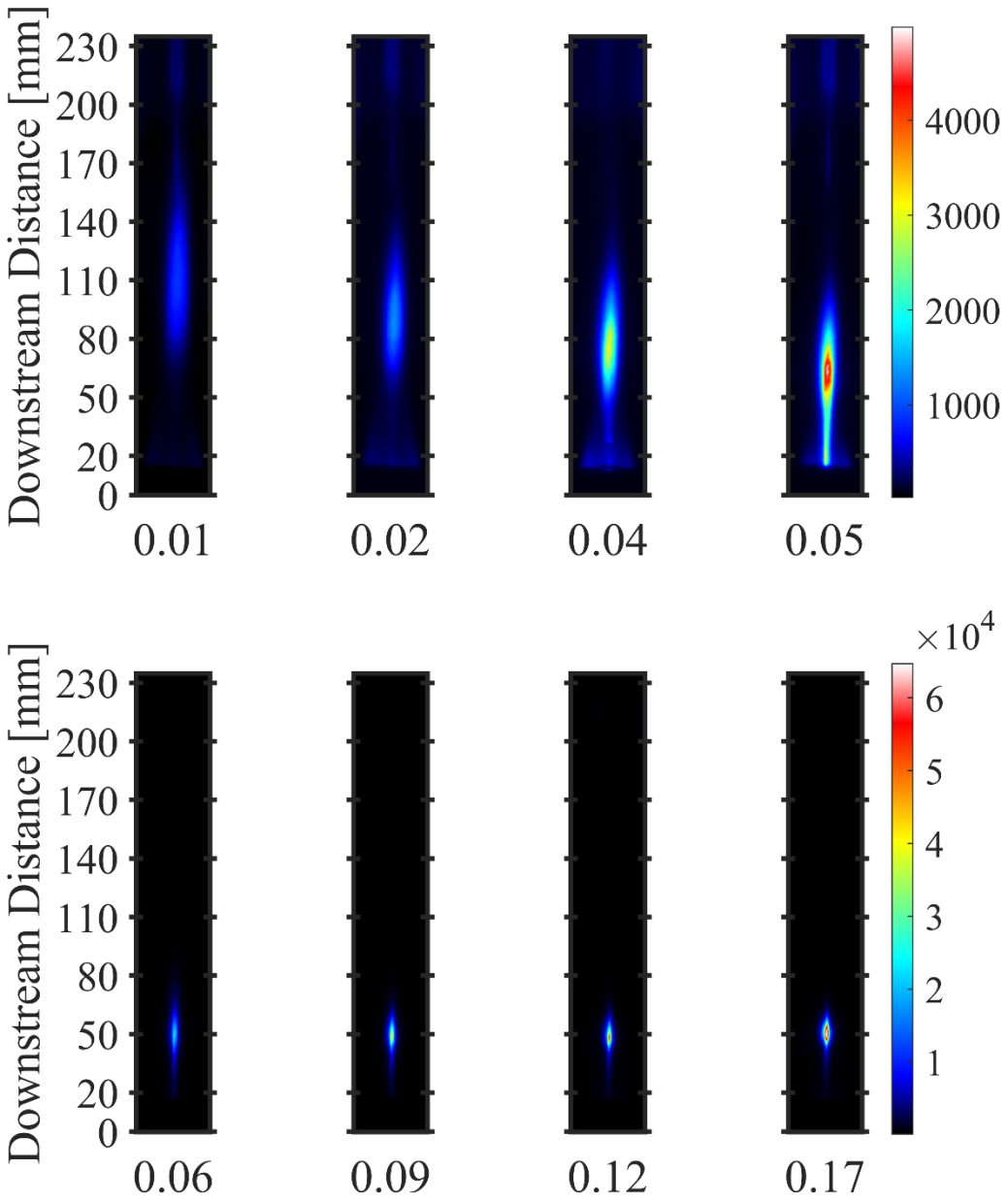

Figure 10. Time-averaged images of CH* chemiluminescence at different O_2 mole fractions under O_2/N_2 environment while T_{ad} is constant.

The four length-scale metrics used to characterize the combustion zones from CH* chemiluminescence imaging are: ignition location (x_1), peak location, FWHM of the CH* signal (x_2-x_1), and volatile burning end location (x_2). These quantities describe the spatial distribution of key processes in the combustion of solid fuels. The ignition location indicates the point where volatile gases have ignited. The peak location indicates the location of most intense volatile

burning. The FWHM of the CH* chemiluminescence signal is an indication of the region over which volatile gases are burnt. Finally, the end of the volatile burning indicates the location where the intense combustion processes have concluded. The results of these four locations for various mixtures of O_2/N_2 with constant T_{ad} are shown in Figure 11.

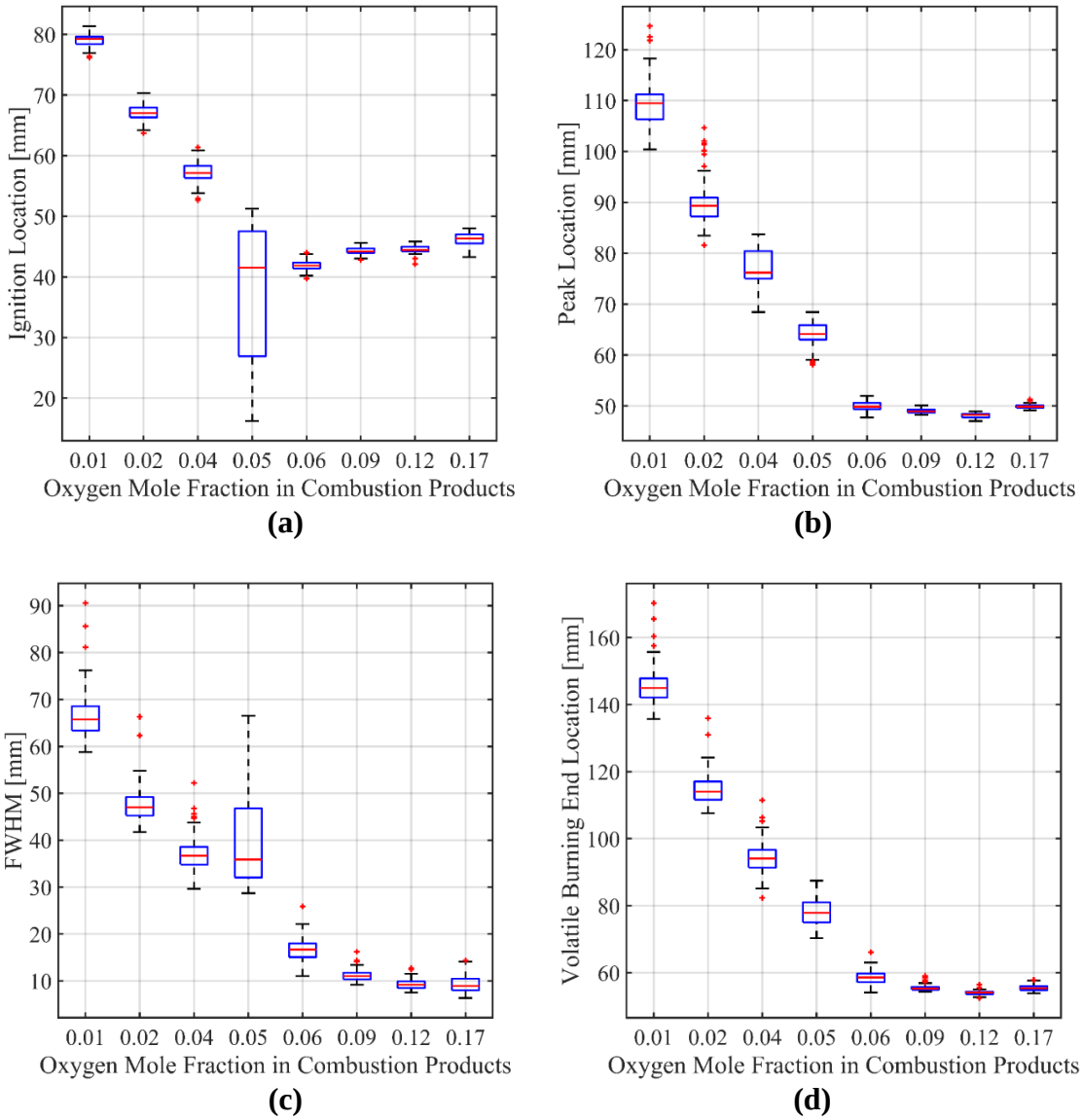

Figure 11. Boxplots for (a) ignition location, (b) peak location, (c) FWHM, and (d) volatile burning end location different O_2 concentrations under O_2/N_2 environment with constant T_{ad} = 1645 K.

Figure 12 shows the time-averaged CH* chemiluminescence images for the constant-oxygen mole fraction test matrix, where temperature of the surrounding gases is varied. The centerline profiles of these time-averaged images are shown in Figure 7 of the main manuscript.

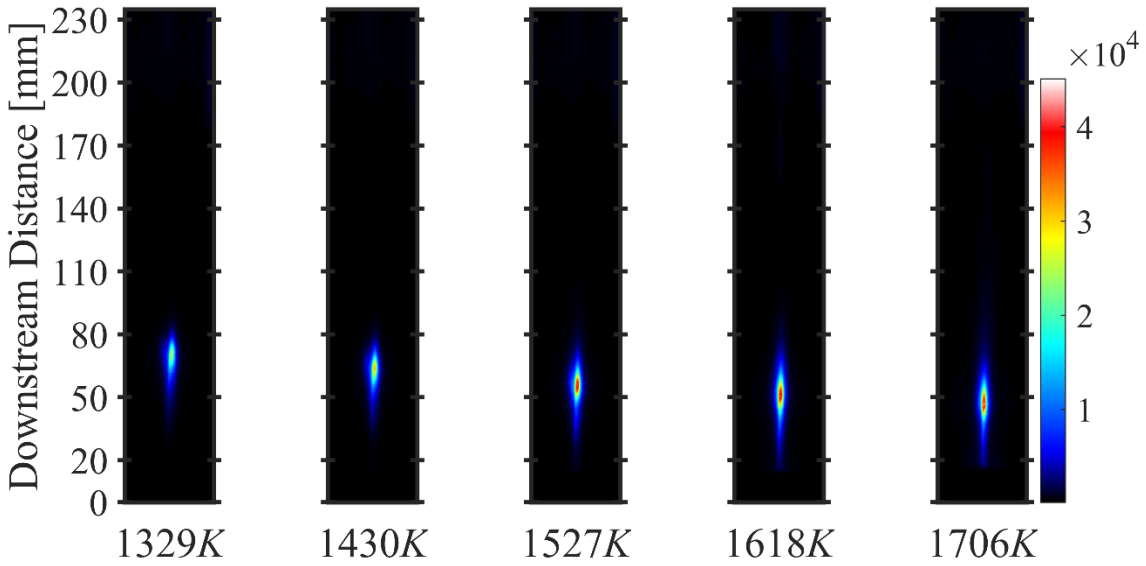

Figure 12. Time-averaged CH* chemiluminescence images at different temperatures under O_2/N_2 environment while O_2 mole fraction in the combustion products is constant.

The effect of adiabatic flame temperature variation on the four length-scale metrics is illustrated in Figure 13. Over the selected temperature range, increasing temperature decreases ignition location, peak location, and volatile burning end location, resulting in accelerated ignition processes. However, the FWHM is not notably affected by the surrounding hot temperature despite changes in the adiabatic flame temperature from 1329K – 1706 K over this operating range.

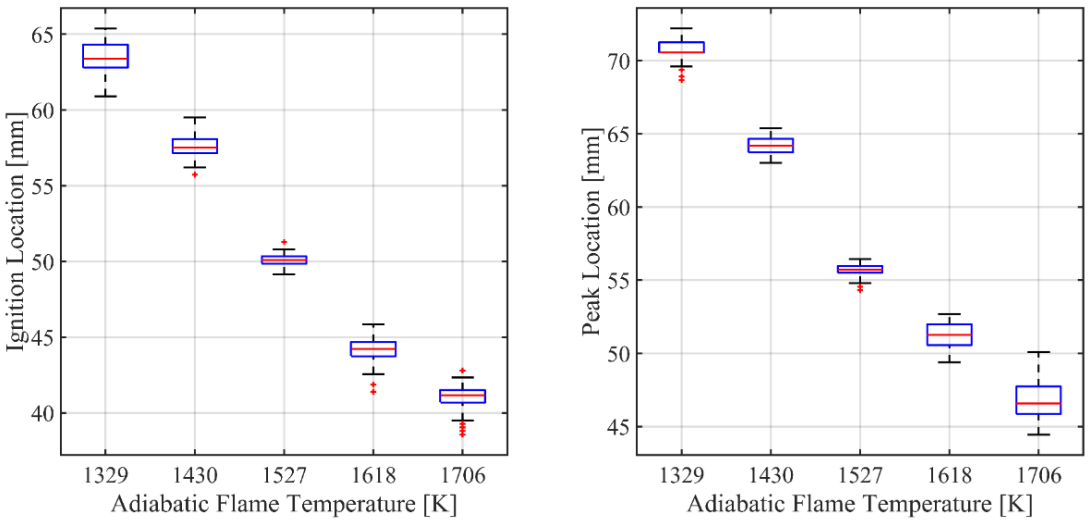

(a) **(b)**

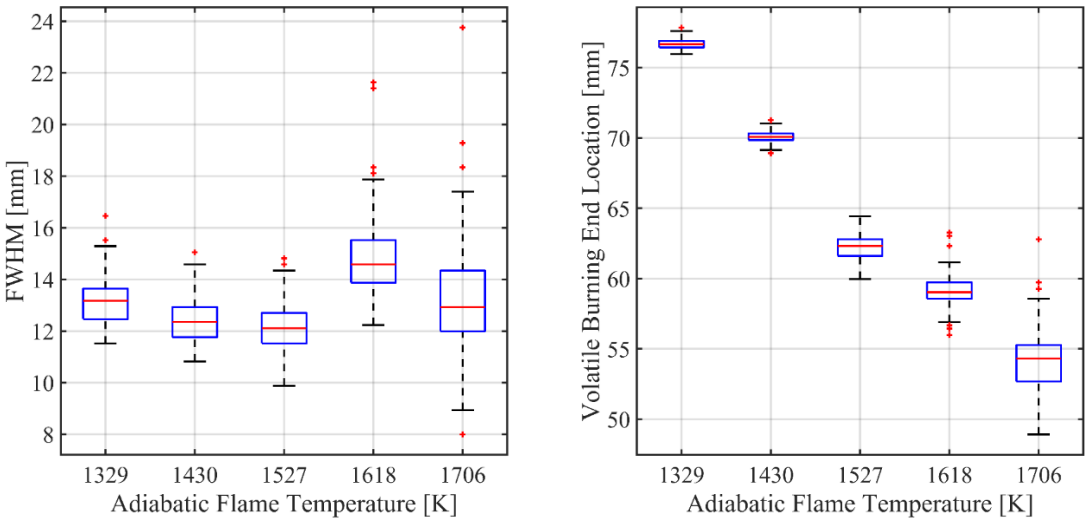

Figure 13. Boxplots for (a) ignition location, (b) peak location, (c) FWHM and (d) volatile burning end location at different O_2 concentrations under O_2/N_2 environment while O_2 concentration in combustion product is constant.

6 Ignition delay time sensitivity study

Ignition delay times of the volatile gases from cellulose were estimated to understand the dependence of rate-limiting processes on the surrounding gas temperature and oxygen mole fraction. However, there is a high level of uncertainty in the composition of the volatile gases. In order to understand the sensitivity of the ignition delay time calculations to the composition of the volatile gases, ignition delay times were computed for three mixtures in addition to the baseline mixture presented in the paper. Table 1 shows an overview of the mixtures. The methodology for choosing the baseline mixture is outlined in the main manuscript. Three additional mixtures were created to test the sensitivity of the ignition delay time to the three "fuels" in the volatile mixture – H_2, CH_4, and C_2H_6. In each case, the mole fraction of the target species was increased by a factor of 2-3 and then the remaining mole fractions were renormalized to reduce the number of variables changing in each simulation. These mixtures are not meant to be representative of any physical mixture, but instead are used to determine the sensitivity of the ignition delay time to volatile composition over the range of operating conditions considered in this study.

Table 1. Volatile composition variation for ignition delay sensitivity study.

Species	Baseline	High H_2	High CH_4	High C_2H_6
H_2	0.080842264	0.178706	0.066904	0.080321
N_2	0.512601743	0.458025	0.424224	0.509293
CH_4	0.091673138	0.081913	0.248277	0.091081
H_2O	0.022832843	0.020402	0.018896	0.022685
C_2H_6	0.003504110	0.003131	0.002900	0.009935
O_2	0.003426782	0.003062	0.002836	0.003405
CO_2	0.285119119	0.254762	0.235962	0.283279

Figure 14 shows the results of this sensitivity analysis, where Figure 14a shows the results for the constant-temperature test matrix, Figure 14b shows the results for the constant-O_2 mole fraction test matrix, and Figure 14c shows the results for the H_2/air test matrix. In all these cases, the composition of the volatile mixture changes the ignition delay times but not dramatically, such that the order-of-magnitude remains the same. Generally, the addition of CH_4 increases ignition delay times or prohibits ignition at very low-oxygen concentrations, which is consistent with previous ignition studies[1]. Similarly, the addition of H_2 decreases ignition delay time, also consistent with previous ignition studies[2]. Despite these differences, the variation in volatile mixture does not dramatically change the estimates of ignition delay time for the purposes of the scaling analysis.

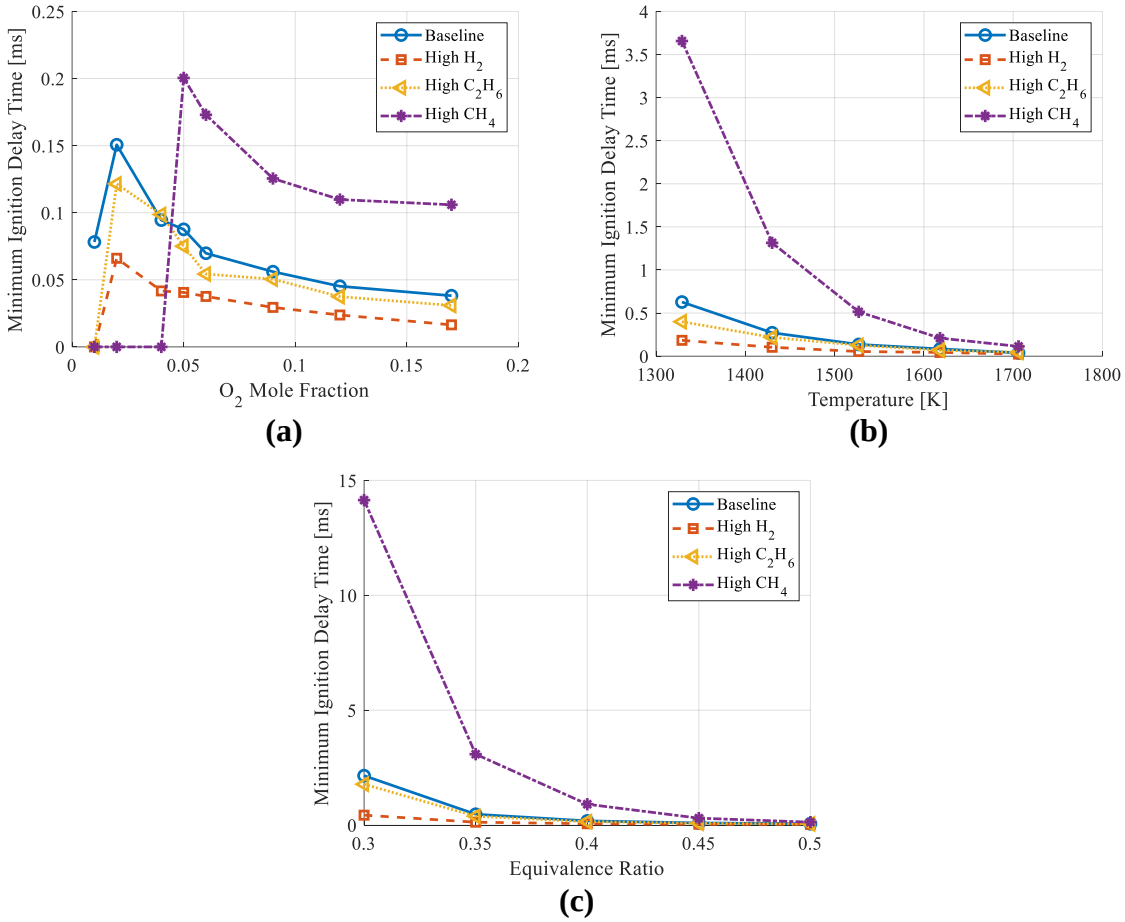

Figure 14. Ignition delay calculations for four volatile mixtures at conditions for the (a) constant-temperature, (b) constant-O_2 mole fraction, and (c) H_2/air test matrices.

[1] Spadaccini, L. J., & Colket, M. B. (1994). "Ignition delay characteristics of methane fuels." *Progress in Energy and Combustion Science*, 20(5), 431-460.

[2] Donohoe, N., Heufer, A., Metcalfe, W. K., Curran, H. J., Davis, M. L., Mathieu, O., Plichta, D., Morones, A., Petersen, E. L., & Güthe, F.. (2014) "Ignition delay times, laminar flame speeds, and mechanism validation for natural gas/hydrogen blends at elevated pressures." *Combustion and Flame*, 161(6), 1432-1443.

7 Ignition delay time calculation using the maximum intensity gradient

In the main paper, the ignition delay time is defined by calculating the full-width half-max of the time-averaged CH* chemiluminescence centerline intensity signal and then using the left-hand extreme of that quantity as the measure of ignition delay location. A second method was tested to determine whether another metric for ignition delay time produced the same results. This method uses the location of the maximum intensity gradient along the rise of the centerline time-averaged CH* chemiluminescence signal as the ignition location. The rest of the procedure in calculating the ignition delay time and uncertainty analysis is similar to the method described in Sections 2.2.3 and 2.2.4. Results for O_2/N_2 mixtures for two cases of different T_{ad} while O_2 mole fraction in combustion products is constant and the case of different O_2 mole fractions while T_{ad} is constant are shown in Figure 15. The dependence of ignition delay time on adiabatic flame temperature and O_2 mole fraction are very similar to the results calculated by FWHM method. For the case of varying O_2 mole fraction in combustion products, the uncertainty bars for the two conditions with lowest O_2 mole fraction is higher. The reason is that in the CH* emission signals in this low oxygen regime are much noisier compared to other conditions, which generates higher uncertainty in locating the point with the maximum intensity gradient.

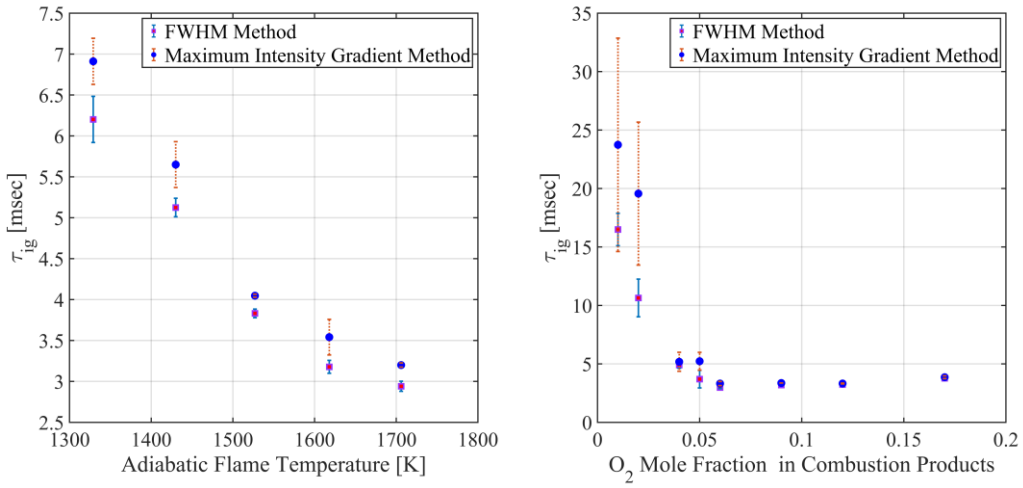

Figure 15. Ignition delay time of microcrystalline cellulose particles vs. (a) different T_{ad} while O_2 mole fraction is constant (b) different O_2 mole fractions while T_{ad} is constant.